DEVELOPMENTS ON THE BOSTON 256-CHANNEL RETINAL IMPLANT

Shawn K. Kelly[1,2], *Member, IEEE*, Douglas B. Shire[1,3], *Member, IEEE*, Jinghua Chen[4], Marcus D. Gingerich[3], Stuart F. Cogan[5], *Member, IEEE*, William A. Drohan[6], *Member, IEEE*, William Ellersick[7], Ashwati Krishnan[2], Sonny Behan[8], John L. Wyatt[6], *Senior Member, IEEE*, and Joseph F. Rizzo III[4]

[1]Department of Veterans Affairs; [2]Carnegie Mellon University, Pittsburgh, PA; [3]Cornell University, Ithaca, NY; [4]Massachusetts Eye and Ear Infirmary, Boston, MA; [5]EIC Laboratories, Norwood, MA; [6]Massachusetts Institute of Technology, Cambridge, MA; [7]Analog Circuit Works, Sudbury, MA; [8]Sonny Behan Consulting, Atlanta, GA
skkelly@cmu.edu

ABSTRACT

A hermetic neurostimulator is being developed to restore functional sight to the blind. The latest developments are presented on the Boston 256-channel retinal prosthesis. The device includes a hermetic package made of titanium and alumina, containing an integrated circuit chip with 256 independently addressable current drivers. The prosthesis attaches to the outside scleral wall of the eye and electrically drives a microfabricated thin-film polyimide array of sputtered iridium oxide electrodes. This array is implanted in the subretinal space via a flap in the sclera. The implanted device receives power and stimulation data wirelessly via inductively coupled coils. A circuit to prevent residual electrode voltage and improve safety is being designed for incorporation into future devices. The components of our prosthesis have been tested, and we plan to implant the 256-channel device in animals this year.

Index Terms— Biomedical engineering, biomedical electrodes, integrated circuit design, retinal prosthesis.

1. INTRODUCTION

A number of research groups and companies are developing visual prostheses for the blind [1]-[8]. Such devices are designed to restore some useful functional vision to patients with degeneration of the outer retina. In particular, age-related macular degeneration is the leading cause of blindness in the developed world, with between 2 million and 9 million cases in the US, and retinitis pigmentosa is the leading cause of inherited blindness, with over 100,000 cases in the US. Many retinal prostheses work by collecting images with a camera, downsampling those images to a small number of pixels while selecting for image saliency, transmitting those data to an implant on the patient's eye, and electrically stimulating the patient's remaining healthy retinal ganglion cells based on the image data to produce some representation of the visual world.

In recent years, a few groups have progressed with clinical trials in blind patients, proving the concept of the retinal prosthesis by demonstrating that visual percepts can be elicited with safe levels of electrical stimulation, that simple visual tasks can be performed, and that restoration of vision can be achieved over a small area of retina with an acuity of about 20/1000. The most advanced prosthesis with individually-addressable electrodes is the Argus II from Second Sight, with 60 stimulating channels [4]. One patient receiving an implant from Retina Implant AG in Germany (with 1500 non-configurable "pixels" made from photodiodes and electrodes) was able to read large text one week after implantation [6], with similar visual function results from other groups. While the results of these early clinical trials are encouraging, they do not represent natural, high-resolution vision, and challenges remain. For example, some amount of head movement is required to scan an image or visual scene, and patients can take as long as tens of seconds to process the information. The drive for higher-resolution vision has motivated our group and others to develop advanced retinal prosthesis devices [7]-[8]. Our own short-term retinal stimulation trials on blind volunteers [9] provided the proof of concept needed to proceed with the design of a chronically implantable device. We report here on the developments on the Boston retinal implant, with over 256 independent stimulating channels.

2. SYSTEM DESIGN

Our retinal prosthesis device includes both external and implanted elements, and is similar in function to the Argus II device. The external components presently include a computer with a graphical user interface that allows a user to select parameters for stimulation. These parameters are

Funding provided by the Department of Veterans Affairs, NIH EY016674-01, Department of Defense, and NSF's support of the Cornell Nanoscale Science and Technology Facility. MOSIS provided in-kind foundry services.

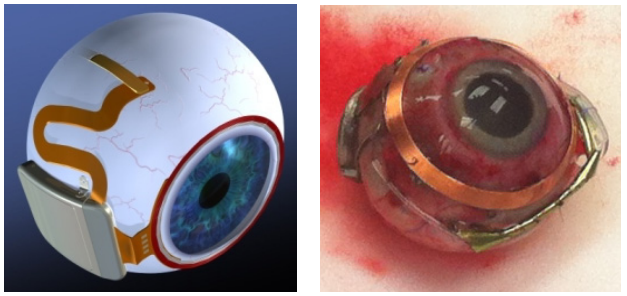

Fig. 1. Retinal implant concept (left), and the 256-channel Boston retinal implant on an enucleated human eye (right). The device is attached to the outside of the eye, sutured to the sclera, the white wall of the eye. The secondary telemetry coil surrounds the cornea, and the entire device sits behind the conjunctiva, the protective membrane of the eyelid. The microelectrode array is inserted through scleral flap into the subretinal space.

converted to digital control data, which are used to modulate a power transmitter. These data, as well as external power, are delivered wirelessly to the implant by inductive coupling. At a later date, a camera and portable image processor will be added to enable clinical trials. The wireless signals and power are received by a custom integrated circuit enclosed in a hermetic titanium case. The chip interprets the data and delivers current to the tissue through 256 independently-controlled channels via a thin-film microfabricated electrode array, terminating in electrodes coated in sputtered iridium oxide film (SIROF).

The retinal implant concept is shown in Figure 1, along with a prototype of our 256-channel device. The implant fits on the outside of the eye and is sutured to the tough sclera that forms the outermost wall of the eye. All of the implanted components sit behind the conjunctiva, the thin membrane attached to the eyelids that overlays the sclera. The electrode array is inserted into the eye through a flap in the sclera, passes through an incision in the choroid, and rests in the subretinal space (as opposed to the Argus II's epiretinal electrode), between the retina and the choroid, where it delivers stimulus current to the retinal nerves.

2.1. Telemetry System Design

The power source for the implant and the data that determine which electrode to drive with which level of current arrive via a near-field inductive link. Sinusoidal currents are driven through an external coil (which will be integrated into a pair of glasses that the patient will wear), creating a sinusoidal magnetic field [10]. This field induces a sinusoidal voltage in an implanted secondary coil, and this voltage is rectified to produce the implant's power supply. Modulations in the drive current encode data in the magnetic field, which can be decoded by the implanted chip. Changes made by the chip to the impedance of the secondary coil are reflected back to the external transmitter circuit and decoded as outbound data. The inbound data include stimulation current values, phase durations, and

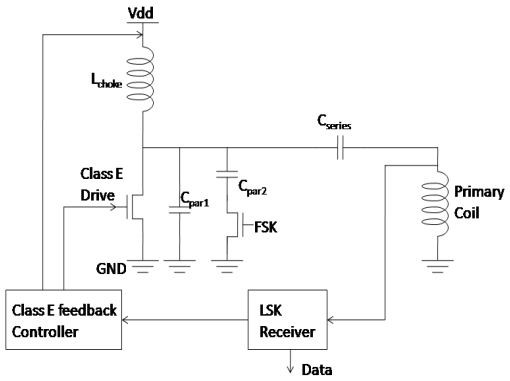

Fig. 2. Class E power transmitter circuit, with an FSK transmitter and an LSK receiver.

other information needed to stimulate each electrode, as well as other control signals. The outbound data include status information, electrode voltage waveforms, implant power supply voltage, and other information needed to support the operation and debugging of implanted devices or lab experiments.

The power and data transmitter circuit is made using a class E power amplifier architecture [11], as shown in Figure 2. The class E transistor switch alternates between ramping up the flux in the choke inductor and sending that current through the tuned inductor-capacitor load that includes the primary transmitting coil. The efficiency of this switching circuit allows amplification of a small DC supply voltage to a large AC voltage on the primary coil. The frequency shift-keying (FSK) transistor switch changes the resonant frequency of the inductor-capacitor load, allowing for discrete modulation of the magnetic field to encode data. Sensing and analysis of the coil voltage allows for reception of load shift-keying (LSK) signals sent out from the implanted device. The class E circuit creates a carrier field at 6.78 MHz, transmitting up to 30 mW of power, encodes FSK data at 565 Kbps, using 8b/10b digital encoding, and receives LSK encoded data from the chip at 47 Kbps. Our class E circuit is shown in Figure 3. The primary coils are made with 8 turns of copper 36 AWG magnet wire, with a radius of approximately 23.6 mm, for an inductance of approximately 11 μH. Our implanted secondary coils are made with 10 turns of gold 40 AWG

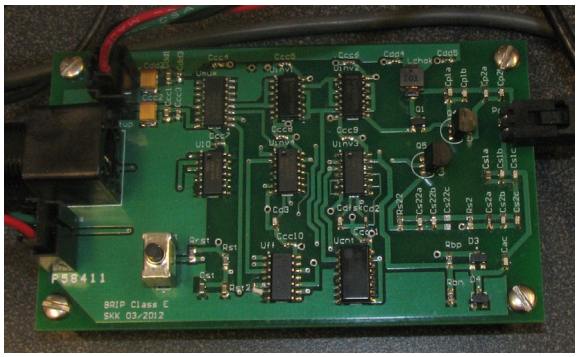

Fig. 3. Our class E power transmitter with FSK modulation.

wire, wound on a 1-inch diameter (12.7 mm radius) spherical mandrel, with an inner diameter of 9.75 mm (for a mean coil radius of roughly 9.9 mm), and have an inductance of approximately 5.5 µH. The self-resonant frequency of each of these coils is well above 6.78 MHz, allowing for tuning with added capacitance.

2.2. Integrated Circuit Design

The central element of the retinal prosthesis is the custom-designed chip that receives data, stimulates retinal tissue using a biphasic constant current drive with multiple redundant safety features, and transmits status data out to the external components [12]. Figure 4 shows a block diagram of our chip. The upper left corner shows the reference circuits that set various chip voltages, as well as the bias current for the current source stimulators. The PWR block regulates the on-chip voltage supplies, while the XMT and RCV blocks transmit and receive data to and from the external circuits by LSK and FSK, respectively. The control logic block includes synthesized circuits that use the received data to control the current drivers on the chip (DRV) and that manage the collected data to be transmitted to the outside. The remaining circuitry is devoted to testing and safety, and includes electrode voltage monitors, on-chip analog test multiplexors, data converters, and memory. Safety features on the chip include stimulus charge limits, data transmission 32-bit CRC error checking, configuration pins to lock out stimulation settings that are not desired, and comprehensive self-test and electrode monitoring. In particular, the chip measures the electrode voltage during the inter-phase interval to ensure that the peak electrode-tissue interface voltage does not exceed a pre-determined value (set inside the water dissolution voltage window) and again measures the electrode voltage after the end of the biphasic pulse, when the electrode has been shorted to the current return for a minimum required amount of time, to determine whether the shorting mechanism is working.

The chip is capable of delivering currents in 1 µA steps up to 127 µA, for durations in 17.7 µs steps up to 4500 µs, subject to total charge limits of 50, 100, or 200 nC, accounting for variations in electrode sizes. Any subset of up to 32 electrodes can be driven in a given stimulus cycle,

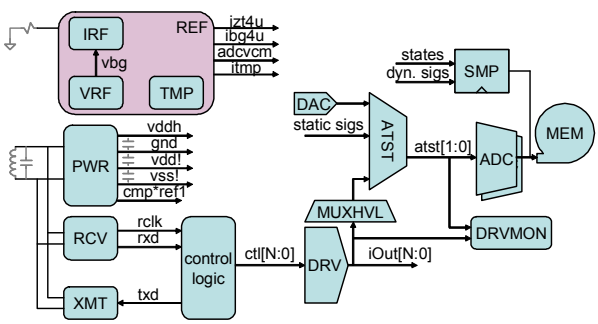

Fig. 4. Block diagram of the Boston retinal implant chip.

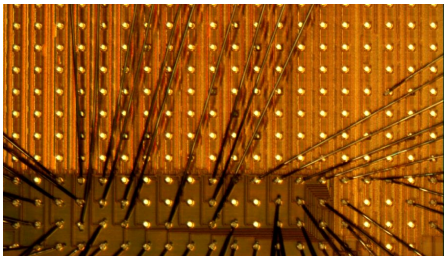
Fig. 5. Boston retinal implant chip, showing some of the 256 electrode current drivers, as well as digital and analog circuits.

at a repetition rate of up to 400 Hz, and electrodes can be configured as current sources or as current sinks to provide current steering capabilities. A micrograph of the retinal implant chip is shown in Figure 5. The die was fabricated by MOSIS in a 0.18 µm high voltage process.

2.3. Residual Voltage Prevention Circuit

While we are developing a true charge-balanced biphasic current source stimulator for clinical trials with the Boston retinal implant, we are also working to develop a novel method of neural stimulation that prevents the creation of residual voltage on an electrode at the end of a biphasic pulse [13]. It is a widely-held misconception that a perfectly charge-balanced biphasic current pulse will result in zero charge and voltage on the electrode at the end of the pulse. However, as is shown in [13] and [14], the leakage through the charge transfer resistance that is in parallel with the electrode capacitance is nearly unidirectional during the pulse, giving a residual positive charge for a negative-first biphasic pulse. This DC voltage can cause damage to the electrodes and to tissue over a long time [15].

To prevent this residual voltage from occurring, we have designed a benchtop stimulator with a feedback loop that corrects the duration of the second phase of stimulation based on the residual voltage recorded after the previous pulse. Other papers have suggested methods of eliminating the residual electrode voltage, either by adding additional brief pulses of negative current until the voltage is eliminated [15] or by applying a DC bias in the opposite direction [16]. However, we wish to avoid adding a DC bias and prefer to prevent the residual voltage from happening in the first place.

In addition to a biphasic stimulator with carefully-controllable phase durations, we designed a sample and hold amplifier to measure the residual voltage at some time after the second phase (we chose 100 µs). This measurement was

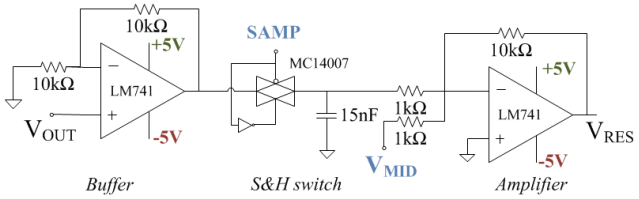

Fig. 6. Sample and hold amplifier circuit

analyzed by a microcontroller to enact the feedback. The sample and hold amplifier circuit is shown in Figure 6.

2.4. Hermetic Enclosure Design

To protect the implanted circuits in the body, we have developed a hermetic enclosure made of titanium and alumina ceramic, with 256 individual electrical feedthroughs [17]. The ceramic feedthrough includes punched holes filled with biocompatible conductive material and is co-fired and then brazed to the roughly 11mm diameter circular titanium case. A small circuit board (10.6 mm in diameter) is assembled with the chip and a small number of resistors, capacitors, and diodes and is attached to the inside surface of the feedthrough by reflowing solder bumps on the feedthrough pads. The titanium case is laser welded shut in a helium environment to enable hermeticity testing, and the electrode array is attached to the outside of the case by thermosonic bonding between gold surfaces electroplated onto both the array and the outside of the feedthrough. Finally, a molded polyurethane header is added on top of the array connections and underfilled with epoxy. The feedthrough and hermetic package are shown in Figure 7. We expect this device to function in the body for at least the five years recommended by the FDA, with a target of ten years. The device is meant to be explantable at the end of its life or in case of complications.

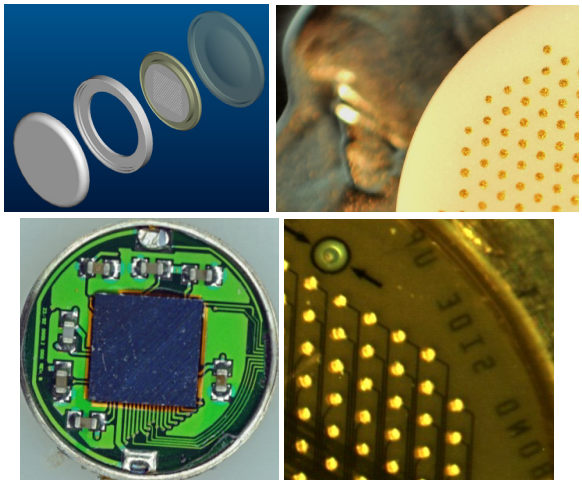

Fig. 7. Hermetic case assembly. Top left, an exploded view of the case; top right, a view of the feedthrough on a nickel; bottom left, circuit board and chip inserted into the case; bottom right, electrode array bonded to the outside of the feedthrough.

2.5. Electrode Array Design

The stimulating currents enter the tissue via a 256-channel thin-film microfabricated electrode array. This array, 15 µm thick, is fabricated with conducting metal sandwiched between insulating layers, as shown in Figure 8. Outer layers of polyimide provide biocompatibility, flexibility, and some ruggedness during surgical insertion. A sandwich of silicon carbide provides a water vapor barrier, enclosing gold wires with titanium adhesion layers. The electrode sites are etched to the gold layer, and then a sputtered iridium oxide film is applied [18], [19].

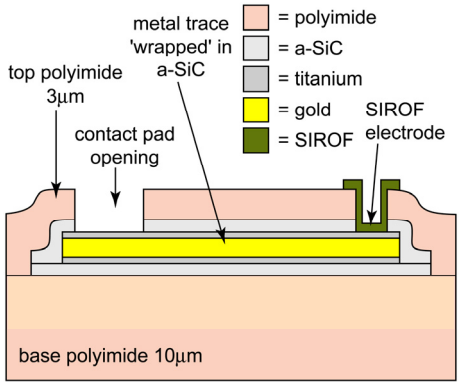

Fig. 8. Electrode array fabrication. A base polyimide layer is spun onto a host wafer. Silicon carbide provides a water vapor barrier. Titanium provides an adhesion layer for gold conductors. Top layers of SiC and polyimide are etched down to the metal, and sputtered iridium oxide film is deposited on the electrodes.

3. RESULTS

Our device and its components were tested both in the lab and *in vivo* in the Yucatan minipig.

3.1. Telemetry System Testing

The power and data communication system was tested in the lab, in conjunction with the transceiver portions of the chip. Figure 9 shows results of this testing. The top graph shows the secondary coil voltage during simultaneous FSK and LSK. The bottom graph shows the inbound telemetry, with the top trace showing the chip's sampling clock, the middle trace showing the received data, and the bottom trace showing the data at the external transmitter board.

3.2. Integrated Circuit Testing

The chip was tested in a bench setup, driving a series resistor and capacitor load as a mock electrode. Selected pads on the chip were wire-bonded to a package, and the chip was interfaced in both wired and wireless fashion. 16 of the stimulation channels were tested in this way, with the remainder to be tested when the implant construction is completed. Figure 10 shows a typical output of a biphasic (positive-first) current pulse being driven through the mock load, with a digital control signal that shorts the electrode to the current return node after the pulse.

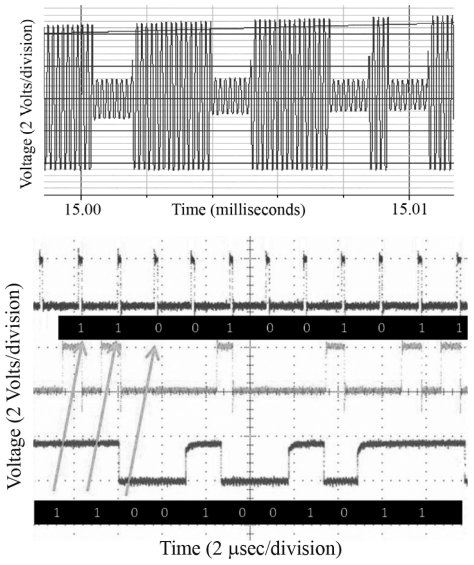

Fig. 9. Top: Secondary coil voltage during simultaneous FSK and LSK modulation. Bottom: Inbound telemetry reception at the chip.

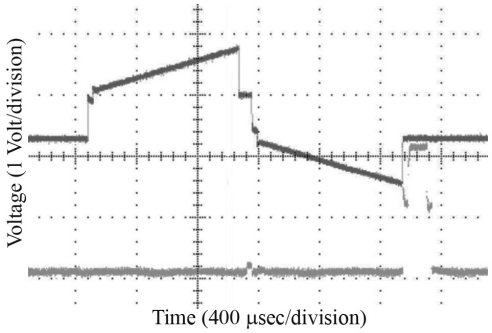

Fig. 10. Current drive through a mock electrode. Top: voltage across a series RC load being driven by a biphasic, positive-first current pulse. Bottom: digital control signal to short the electrode to the current return after the pulse.

The chip area is roughly 5mm × 5mm, and standby power consumption is approximately 0.1 mW, with 30% efficiency during stimulation.

3.3. Residual Voltage Circuit Testing

In residual voltage testing experiments, the electrode voltage was measured 2 ms after the second pulse, and the measurement window spanned 10 µs. After 10 seconds of pulsing, the feedback system was enabled, using simple proportional feedback with k = 1000 s/V. Figure 11 shows the results of the feedback system. The first 10 seconds of the trace in the figure show the residual voltage that exists on the electrode without feedback, using equal negative and positive phase widths. The rest of the trace shows that the residual voltage is driven to nearly zero when the feedback is enabled. The average duration of the second phase when feedback is enabled is 916 µs, since less positive current is needed because the residual voltage is positive.

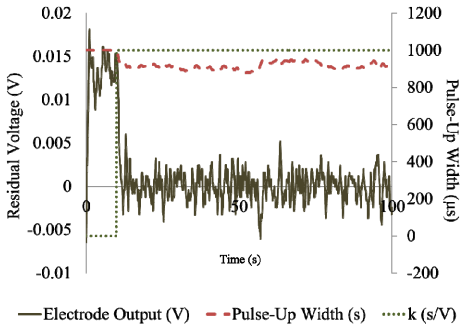

Fig. 11. Effect of second-phase feedback on residual voltage at the end of a biphasic stimulus pulse. The upper trace shows the duration of the second phase.

3.4. Hermetic Package Testing

The co-fired ceramic feedthroughs were tested for helium leakage, and measured for hermeticity. A helium leak rate of between 10^{-9} and 10^{-8} standard cc/sec was measured across the devices. The moisture leak rate is typically about half that of helium, and with the internal volume of our implant, we expect a life of 5-10 years, though more careful helium leak tests need to be performed [20].

3.5. Surgical Implantation

Earlier versions of our device were implanted into seven Yucatan minipigs and continued to function for up to one year [2], [18]. Mockups of the 256-channel device have also been implanted, as shown in Figure 12. The new device is smaller and more conformal than our previous designs, and the mockups have been well tolerated in the minipig eye. We plan to implant assembled, active 256-channel devices for long-term studies in minipigs in 2013.

4. CONCLUSIONS AND FUTURE WORK

The Boston Retinal Implant Project has developed a 256-channel retinal prosthesis for the blind. This device includes the highest density hermetically packaged implant of any type. The integrated circuit and telemetry system are designed and tested, and the hermetic package has been leak tested. We plan to complete the assembly and perform preliminary animal testing in 2013, complete engineering and pre-clinical testing of the devices, and begin clinical trials within the next two years. In addition, we have developed a new circuit for stimulating without residual voltage, which we will incorporate into future chips.

We hope that this device will restore some functional vision to those blinded by degenerative retinal diseases. While the devices currently being developed and tested restore only simplistic vision to a small area of retina with little control over color, we expect future developments to drastically improve the vision restored to blind patients.

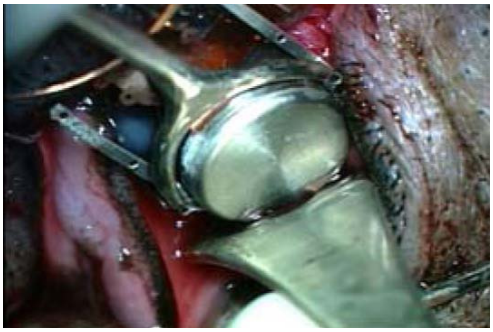

Fig. 12. A mockup 256-channel implant onto a minipig eye.

5. REFERENCES

[1] J.F. Rizzo III, J. Wyatt, M. Humayun, E. de Juan, W. Liu, A. Chow, R. Eckmiller, E. Zrenner, T. Yagi, and G. Abrams, "Retinal prosthesis: an encouraging first decade with major challenges ahead," Ophthalmology, vol. 108, 2001, pp. 13-14.

[2] S.K. Kelly, D.B. Shire, J. Chen, P. Doyle, M.D. Gingerich, S.F. Cogan, W. Drohan, S. Behan, L. Theogarajan, J.L. Wyatt, J.F. Rizzo, "A Hermetic Wireless Subretinal Neurostimulator for Vision Prostheses," IEEE Trans. on Biomedical Engineering, vol. 58, no. 11, 2011, pp. 3197-3205.

[3] N. Alteheld, G. Roessler, P. Walter, "Towards the bionic eye – the retinal implant: surgical, ophthalmological and histopathological perspectives," Acta Neurochi. Suppl., vol. 97(2), 2007, pp. 487-493.

[4] J.D. Weiland, A.K. Cho, M.S. Humayun, "Retinal prostheses: current clinical results and future needs," Ophthalmology, vol. 118, 2011, pp. 2227-2237.

[5] C.D. Eiber, N.H. Lovell, G.J. Suaning, "Attaining higher resolution visual prosthetics: a review of the factors and limitations," J. Neural Eng., vol. 10, no. 1, 2013, 17pp.

[6] E. Zrenner, K.U. Bartz-Schmidt, H. Benav, D. Besch, A. Bruckmann, V.P. Gabel, F. Gekeler, U. Greppmaier, A. Harscher, S. Kibbel, J. Koch, J. Kusnyerik, T. Peters, K. Stingl, H. Sachs, A. Stett, P. Szurman, B. Wilhelm, R. Wilke, "Subretinal electronic chips allow blind patients to read letters and combine them to words," Proc. Biol. Sci., vol. 278, 2011, pp. 1489-1497.

[7] K. Chen, Z. Yang, L. Hoang, J. Weiland, M. Humayun, W. Liu, "An integrated 256-channel epiretinal prosthesis," IEEE J. Solid-State Circuits, vol. 45, 2010, pp. 1946-1956.

[8] N. Tran, E. Skafidas, J. Yang, S. Bai, M. Fu, D. Ng, M. Halpern, I. Mareels, "A prototype 64-electrode stimulator in 65nm CMOS process towards a high density epi-retinal prosthesis," Proc. IEEE Eng. Med. Biol. Soc., 2011, pp. 6729-6732.

[9] J.F. Rizzo, J.L. Wyatt, J. Loewenstein, S.K. Kelly, D.B. Shire, "Perceptual Efficacy of Electrical Stimulation of Human Retina with a Microelectrode Array During Short-Term Surgical Trials," Invest. Ophth. and Visual Science, Vol. 44, No. 12, 2003, pp. 5362-5369.

[10] S.K. Kelly, P. Doyle, A. Priplata, O. Mendoza, J.L. Wyatt, "Optimal Primary Coil Size for Wireless Power Telemetry to Medical Implants," IEEE ISABEL Int'l Symposium on Applied Sciences in Biomedical and Communication Tech., 2010.

[11] P.R. Troyk, M.A.K. Schwan, "Closed-loop class E transcutaneous power and data link for microimplants," IEEE Trans. on Biomed. Eng., vol. 39, no. 6, 1992, pp. 589-599.

[12] D.B. Shire, W. Ellersick, S.K. Kelly, P. Doyle, A. Priplata, W. Drohan, O. Mendoza, M. Gingerich, B. McKee, J.L. Wyatt, J.F. Rizzo, "ASIC Design and Data Communications for the Boston Retinal Prosthesis," Proc. IEEE Engineering in Medicine and Biology Conference, 2012, pp. 292-295.

[13] A. Krishnan, S.K. Kelly, "On the Cause and Control of Residual Voltage Generated by Electrical Stimulation of Neural Tissue," Proc. IEEE Engineering in Medicine and Biology Conference, 2012, pp. 3899-3902.

[14] S.F. Cogan, "Neural stimulation and recording electrodes," Annual Review of Biomedical Engineering, vol. 10, 2008, pp. 275-309.

[15] M. Ortmanns, "Charge balancing in functional electrical stimulators: A comparative study," IEEE Int'l Symp. on Circuits and Systems, 2007, pp. 573-576.

[16] K. Sooksood, T. Stieglitz, M. Ortmanns, "An active approach for charge balancing in functional electrical stimulation," IEEE Int'l Symp. on Circuits and Systems, 2009, pp. 341-344.

[17] D.B. Shire, T. Salzer, W. Jones, A. Karbasi, S. Behan, W.A. Drohan, O. Mendoza, J. Chen, J.L.Wyatt, J.F. Rizzo, "Hermetic sealing and packaging technology for the Boston retinal prosthesis," Invest. Ophth. and Vis. Sci. vol. 53, 2012, 5523.

[18] D.B. Shire, S.K. Kelly, J. Chen, P. Doyle, M.D. Gingerich, S.F. Cogan, W. Drohan, O. Mendoza, L. Theogarajan, J.L. Wyatt, J.F. Rizzo, "Development and Implantation of a Minimally-Invasive, Wireless Sub-Retinal Neurostimulator," IEEE Trans. on Biomedical Engineering, vol. 56, no. 10, 2009, pp. 2502-2511.

[19] M.D. Gingerich, D.B. Shire, S.F. Cogan, T. Plante, J.L. Wyatt, J.F. Rizzo, "A Microfabricated Subretinal Electrode Array With an Integrated a-SiC Barrier," Invest. Ophthalmol. Vis. Sci. vol. 51:4, 2010, 3040.

[20] G. Jiang, D.D. Zhou, "Technology Advances and Challenges in Hermetic Packaging for Implantable Medical Devices," in Implantable Neural Prostheses 2: Techniques and Engineering Approaches, D. Zhou, E. Greenbaum, eds., Springer, 2010.